Novel piperonal 1,3,4-thiadiazolium-2-phenylamines mesoionic derivatives: Synthesis, tyrosinase inhibition evaluation and HSA binding study

Natália Drumond Lopes, Otávio Augusto Chaves, Márcia C.C. de Oliveira, Carlos Mauricio R. Sant'Anna, Danilo Sousa-Pereira, José Carlos Netto-Ferreira, Aurea Echevarria

PII: S0141-8130(17)32734-4
DOI: https://doi.org/10.1016/j.ijbiomac.2018.02.050
Reference: BIOMAC 9104

To appear in:

Received date: 25 July 2017
Revised date: 6 February 2018
Accepted date: 7 February 2018

Please cite this article as: Natália Drumond Lopes, Otávio Augusto Chaves, Márcia C.C. de Oliveira, Carlos Mauricio R. Sant'Anna, Danilo Sousa-Pereira, José Carlos Netto-Ferreira, Aurea Echevarria , Novel piperonal 1,3,4-thiadiazolium-2-phenylamines mesoionic derivatives: Synthesis, tyrosinase inhibition evaluation and HSA binding study. The address for the corresponding author was captured as affiliation for all authors. Please check if appropriate. Biomac(2017), https://doi.org/10.1016/j.ijbiomac.2018.02.050

Novel piperonal 1,3,4-thiadiazolium-2-phenylamines mesoionic derivatives: Synthesis, tyrosinase inhibition evaluation and HSA binding study

Natália Drumond Lopes,† Otávio Augusto Chaves,† Márcia C. C. de Oliveira, Carlos Mauricio R. Sant'Anna, Danilo Sousa-Pereira, José Carlos Netto-Ferreira,* Aurea Echevarria,*

Departamento de Química, Universidade Federal Rural do Rio de Janeiro, BR-465 Km 7, 23970-000 Seropédica-RJ, Brazil.

† These authors contributed equally to this work

*jcnetto.ufrrj@gmail.com (J.C.N-F.); echevarr@ufrrj.br (A.E.)

Abstract

A novel series of piperonal mesoionic derivatives (**PMI 1-6**) was synthesized. Tyrosinase inhibition in the presence of **PMI-1, -2, -3, -4, -5** and **-6** as well as human serum albumin (HSA) binding studies with **PMI-5** and **PMI-6** were done by spectroscopic and theoretical methods. The mesoionic compound **PMI-5** is the most promising tyrosinase inhibitor with a noncompetitive inhibitory mechanism and an IC_{50} = 124 μmol L^{-1}. In accordance with the kinetic profile, molecular docking results show that **PMI-5** is able to interact favorably with the tyrosinase active site containing the substrate molecule, L-DOPA, interacting with Val-247, Phe-263 and Val-282 residues. The spectroscopic results for the interaction HSA:**PMI-5** and HSA:**PMI-6** indicated that these mesoionic compounds can associate with HSA in the ground state and energy transfer can occur with high probability. The binding was moderate, spontaneous and can perturb significantly the secondary structure of the albumin. The molecular docking results suggest that **PMI-5** and **PMI-6** are able to be accommodated inside the Sudlow's site I in HSA, interacting with hydrophobic and hydrophilic amino acid residues.

Keywords: Mesoionic compounds, tyrosinase, human serum albumin.

1. Introduction

Tyrosinase is the enzyme involved in melanin production and other pigments *via* oxidation reaction of L-tyrosine. It is a dicopper-contained enzyme which catalyzes the melanin synthesis by the action of monophenolase in the hydroxylation reaction of tyrosine and by the diphenolase action in the L-DOPA oxidation to *ortho*-dopaquinone [1]. Tyrosinase plays an important role in medicinal, agricultural and cosmetic fields. Tyrosinase inhibitors are used to treat hyperpigmentation diseases, age spots and skin whitening among others, whereas tyrosinase activators cause the increase of melanogenesis that can protect the skin from UV damage [2]. It has also been suggested that tyrosinase contributes to neurodegeneration processes correlated to Parkinson's disease [3] and, thus, tyrosinase inhibitors has been studied as a possible treatment for this kind of disease.

In recent years, many natural and synthetic compounds that can act as tyrosinase inhibitors or activators have been reported [4-6]. However, only a few of them are in clinical use. Thus, new investigations are necessary to lead to the discovery of novel compounds with activity towards this enzyme. In searching for new synthetic compounds with anti-tyrosinase activity the 1,3,4-thiadiazolium class was chosen because some other heterocyclic compounds, such as thiazoles [7], oxazolones [8], pyrazoles [9], and triazolothiadiazoles [10], have shown interesting effects against tyrosinase.

The 1,3,4-thiadiazolium-2-phenylamine chlorides are precursors of mesoionic compounds, a special class of heterocyclic compounds with diverse biological activities, such as anti-inflammatory, analgesic [11,12], antibacterial, antifungal [13,14], antiparasitic [15,16] and antitumor [17-19]. These mesoionic compounds possess a positive charge in the heterocyclic ring and contain a negatively charged atom on the exocyclic group; however, their overall neutrality allows them to cross biological membranes and to interact with biomolecules such as proteins and DNA [20].

Human serum albumin (HSA) is the most abundant carrier and well-known protein in the human circulatory system. HSA is composed of three structurally similar domains, *i. e* I-III, and each domain consists of two subdomains (A and B) stabilized by 17 disulfide bridges [21]. Besides, HSA contributes to the osmotic blood pressure and can play a dominant role in transportation, disposition and efficacy of many biologically active compounds in the circulatory system [22]. A crucial fact is that drugs and bioactive small molecules bind reversibly to albumin and by consequence the study of the interaction of potential drugs with this protein is extremely important.

The interesting structure of the 1,3,4-thiadiazolium-2-phenylamine class of compounds and the promising therapeutic applications therefrom led us to synthesize a new series of such compounds (Figure 1). In the present work, the synthesis and characterization of novel piperonal 1,3,4-thiadiazolium-2-phenylamine mesoionic derivatives were described, as well as the experimental and theoretical evaluation of their action as tyrosinase inhibitors. In order to understand their transportation and delivery ability following interaction with HSA, the two best tyrosinase inhibitors, namely **PMI-5** and **PMI-6**, were investigated under physiological conditions (PBS solution, pH = 7.4) at 296 K, 303 K and 310 K by spectroscopic techniques (fluorescence and circular dichroism) and molecular docking.

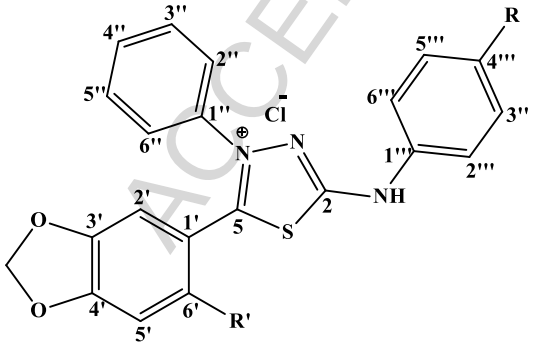

PMI-1 R = H, R’ = H
PMI-2 R = H, R’ = NO_2
PMI-3 R= H, R’ = Br
PMI-4 R = NO_2, R’ = H
PMI-5 R = Cl, R’ = H
PMI-6 R = Br, R’ = H

Figure 1. Chemical structure and code of the synthetic piperonal 1,3,4-thiadiazolium-2-phenylamine mesoionic derivatives.

2. Experimental

2.1. General

Melting points were recorded on a Mel-Temp II capillary melting point apparatus and were not corrected. IR spectra were recorded on a Bruker Vertex 70 spectrophotometer using potassium bromide tablets. ^{1}H and ^{13}C NMR spectra were obtained in a Bruker NMR Ultrashield 400 MHz spectrometer, with tetramethylsilane as the internal reference and DMSO-d_6 as the solvent. Elemental analyses were performed on a PerkinElmer 2400 CHN in the Laboratory of Environmental Science at *Universidade Estadual do Norte Fluminense* (UENF). Reactions were monitored by TLC on Merck silica-gel 60 F254. TLC spots were visualized by inspection of the plates under UV light (254 and 365 mm). The microwave-assisted organic reactions were performed in a Consul CM020BFANA, a domestic oven.

L-DOPA, EDTA and mushroom tyrosinase were obtained from Sigma-Aldrich Chemical Company. Formation of dopachrome was determined by monitoring the absorbance at 475 nm with a Shimadzu UV-VIS spectrophotometer UV Mini 1240 (Kyoto, Japan).

Commercially available HSA, warfarin, ibuprofen and PBS buffer (pH = 7.4) were obtained from Sigma-Aldrich Chemical Company. One tablet of PBS dissolved in 200 mL of millipore water yields a 0.01 mol L^{-1} phosphate buffer solution, containing 0.0027 mol L^{-1} potassium chloride and 0.137 mol L^{-1} sodium chloride, pH 7.4, at 298 K. Water used in all experiments was Millipore water. DMSO and methanol (both spectroscopic grade) were obtained from Tedia Ltd.

2.2. Synthesis

2.2.1. General procedure for the microwave-promoted synthesis of 5-(3,4-methylenedioxy-6-R')-1,3,4-thiadiazolium-2-(4-R-phenyl)amine chlorides (**PMI-1** to **PMI-6**):

The 5-(3,4-*methylenedioxy*-6-*R*')-1,3,4-thiadiazolium-2-(4-*R*-phenyl)amine chlorides were synthesized as previously reported [18]. Briefly, the substituted 3,4-methylenedioxy-6-*R*'-

benzaldehydes (0.35 mmol) [23], and the N_1-phenyl-N_4-(4'-*R*-phenyl)-thiosemicarbazides (0.35 mmol) [24] were mixed in the presence of thionyl chloride and few drops of 1,4-dioxane. The mixture was then submitted to microwave irradiation for 5 min in an open vessel. After this time, the mixture was added to 1,4-dioxane and left to stand overnight at room temperature. The obtained products were filtered, washed with ice-cold water and purified by recrystallization from chloroform:ethanol (60:40, v/v).

2.2.2. 5-(3,4-methylenedioxy-phenyl)-1,3,4-thiadiazolium-2-phenylamine chloride (**PMI-1**)

Yellow solid; 92% yield; mp 286-287 °C [25]; IR (KBr) ν / cm^{-1} 3053, 2902, 2642, 1604, 1566, 1498, 1448, 1311, 1242, 754 and 692; ^{1}H NMR (400 MHz, DMSO-d_6) δ 12,37 (s, 1H, NH), 7.72 (m, 2H, H-2'', H-6''), 7.62 (m, 4H, H-3'', H-4'', H-5'', H-2'''), 7.46 (t, 2H, *J* 7.6 Hz, H3''', H5'''), 7.15 (m, 3H, H-5', H6', H4'''), 6.94 (s, 1H, H2'), 6.17 (s, 2H, OCH_2O); ^{13}C NMR (100 MHz, DMSO-d_6) δ 164.4 (C5), 160.6 (C2), 152.7 (C3'), 148.3 (C4'), 138.9 (C1''), 138.3 (C1'''), 131.9 (C4''), 130.9 (C3'''), 130.0 (C3''), 127.0 (C6'), 126.6 (C2''), 124.6 (C4'''), 118.9 (C2'''), 116.5 (C1'), 109.8 (C2'), 109.7 (C5'), 103.2 (OCH_2O).

2.2.3. 5-(3,4-methylenedioxy-6'-nitro-phenyl)-1,3,4-thiadiazolium-2-phenylamine chloride (**PMI-2**)

Yellow solid; 95% yield; mp 264-266 °C [25]; IR (KBr) ν / cm^{-1} 3008, 1602, 1566, 1494, 1450, 1365, 1326, 1267, 752 and 688; ^{1}H NMR (400 MHz, DMSO-d_6) δ 12.75 (s, 1H, NH), 7.95 (s, 1H, H5'), 7.65 (d, *J* 7.6 Hz, 2H, H2'', H6''), 7.58 (m, 5H, H3'', H4'', H5'', H3''', H5'''), 7.46 (t, 2H, *J* 7.9 Hz, H2''', H6'''), 7.19 (t, *J* 7.4 Hz 1H, H4'''), 6.38 (s, 2H, OCH_2O); ^{13}C NMR (100 MHz, DMSO-d_6) δ 163.2 (C5), 161.8 (C2), 152.9 (C6'), 151.7 (C3'), 142.8 (C4'), 138.8 (C1''), 137.5 (C1'''), 132.2 (C4''), 130.6 (C3'''), 130.0 (C3''), 125.6 (C2''), 124.7 (C4'''), 119.0 (C2'''), 114.6 (C1'), 111.2 (C5'), 106.7 (C2'), 105.6 (OCH_2O).

2.2.4. 5-(3,4-methylenedioxy-6'-bromo-phenyl)-1,3,4-thiadiazolium-2-phenylamine chloride (**PMI-3**)

Yellow solid; 90% yield; mp 278-279 °C; IR (KBr) ν / cm^{-1} 3012, 1604, 1568, 1498, 1469, 1244, 748 and 688; ^{1}H NMR (400 MHz, DMSO-d_6) δ 13.00 (s, 1H, NH), 7.64 (m, 7H, H2', H5', H2'', H3'', H4'', H5'', H6''), 7.46 (m, 4H, H2''', H3''', H5''', H6'''), 7.18 (t, 1H, *J* 7.3 Hz, H4'''), 6.21 (s, 2H, OCH_2O); ^{13}C NMR (100 MHz, DMSO-d_6) δ 162.5 (C5), 162.2 (C2), 152.4 (C4'), 148.0 (C3'), 138.7 (C1'''), 137.8 (C1''), 132.1 (C4''), 130.3 (C3''), 130.0 (C2''), 125.8 (C3'''), 124.7 (C4'''), 119.0 (C2'''), 116.7 (C1'), 115.2 (C6'), 113.6 (C5'), 112.2 (C2'), 104.0 (OCH_2O); Anal. calcd. for $C_{21}H_{15}BrClN_3O_2S$: C, 51.60; H, 3.09; N, 8.60. Found: C, 51.73; H, 2.89; N, 8.72.

2.2.5. 5-(3,4-methylenedioxy-phenyl)-1,3,4-thiadiazolium-2-(4''-nitrophenyl)amine chloride (**PMI-4**)

Yellow solid; 89% yield; mp 243-244 °C; IR (KBr) ν / cm^{-1} 2892, 1620, 1539, 1500, 1450, 1330 and 1243; ^{1}H NMR (400 MHz, MeOD) δ 8.34 (d, 2H, *J* 9.0 Hz, H3''', H5'''), 7.83 (d, 2H, *J* 9.0 Hz, H2'', H6''), 7.70 (m, 5H, H3'', H4'', H5'', H2''', H6'''), 7.22 (d, 1H, *J* 8.3, 1.5 Hz, H6'), 7.01 (d, 1H, *J* 8.3 Hz, H5'), 6.87 (s, 1H, *J* 1.5 Hz, H2'), 6.12 (s, 2H, OCH_2O); ^{13}C NMR (100 MHz, MeOD) δ 166.2 (C5), 160.4 (C2),153.0 (C3'), 148.9 (C4'), 143.6 (C4'''), 143.5 (C1'''), 137.9 (C1''), 131.6 (C4''), 130.0 (C3''), 126.9 (C6'), 125.7 (C2''), 125.0 (C3'''), 118.3 (C2'''), 115.6 (C1'), 109.1 (C5'), 108.8 (C2'), 103.1 (OCH_2O); Anal. calcd. for $C_{21}H_{15}ClN_4O_4S$: C, 55.45; H, 3.32; N, 12.32. Found: C, 55.61; H, 3.12; N, 12.43.

2.2.6. 5-(3,4-methylenedioxy-phenyl)-1,3,4-thiadiazolium-2-(4''-chlorophenyl)amine chloride (**PMI-5**)

Yellow solid; 60% yield; mp 309-310 °C; IR (KBr) ν / cm^{-1} 2730, 1616, 1562, 1494, 1469, 1330 and 1240; ^{1}H NMR (400 MHz, MeOD) δ 7,65 (m, 7H, H2'', H3'', H4'', H5'', H6'', H3''', H5'''), 7.44 (d, 2H, *J* 8.8 Hz, H2''', H6'''), 7.18 (dd, 1H, *J* 8.2, 1.9 Hz, H6'), 6.99 (d, 1H, *J* 8.3 Hz, H5'),

6.85 (d, 1H, *J* 1.8 Hz, H2‘), 6.11 (s, 2H, OCH_2O) ; ^{13}C NMR (100 MHz, MeOD) δ 164.8 (C5), 160.8 (C2), 152.8 (C4’), 148.9 (C3’), 138.0 (C1’’’), 137.1 (C1’’), 131.5 (C4’’), 129.9 (C3’’), 129.5 (C6’), 129.2 (C1’), 126.6 (C2’’), 125.6 (C3’’’), 120.2 (C2’’’), 115.9 (C4’’’), 109.0 (C5’), 108.7 (C2’), 103.1 (OCH_2O); Anal. calcd. for $C_{21}H_{15}Cl_2N_3O_2S$: C, 56.77; H, 3.40; N, 9.46. Found: C, 56.81; H, 3.37; N, 9.52.

2.2.7. 5-(3,4-methylenedioxy-phenyl)-1,3,4-thiadiazolium-2-(4’’-bromophenyl)amine chloride (**PMI-6**)

Yellow solid; 65% yield; mp 280-281 °C; IR (KBr) ν / cm^{-1} 3402, 1616, 1562, 1494, 1470, 1330 and 1242; ^1H NMR (400 MHz, DMSO-d_6) δ 12.95 (s, 1H, NH), 7.63 (m, 9H, H2’’, H3’’, H4’’, H5’’, H6’’, H2’’’, H3’’’, H5’’’, H6’’’), 7.11 (d, 2H, *J* 9.8 Hz, H5’, H6’), 6.95 (s, 1H, H2’), 6.16 (s, 2H, OCH_2O); ^{13}C NMR (100 MHz, DMSO-d_6) δ 164.7 (C5), 160.3 (C2), 152.0 (C4’), 148.3 (C3’), 138.3 (C1’’’), 132.8 (C4’’), 131.9 (C3’’), 130.5 (C6’), 127.0 (C2’’), 126.6 (C3’’’), 120.7 (C2’’’), 116.5 (C1’), 116.1 (C4’’’), 109.8 (C5’), 109.7 (C2’), 103.2 (OCH_2O); Anal. calcd. for $C_{21}H_{15}BrClN_3O_2S$: C, 51.60; H, 3.09; N, 8.60. Found: C, 51.74; H, 2.92; N, 8.72.

2.3. Tyrosinase assays

The mushroom tyrosinase activity was determined by the oxidation of L-DOPA (0.17 $mmolL^{-1}$) into dopachrome in a phosphate buffer medium (50 mmol L^{-1}, pH 6.8) in the presence of EDTA (0.022 mmol L^{-1}), tyrosinase (50-100 units) and different concentrations of each of the mesoionic compounds under investigation. All experiments were done in triplicate. Formation of dopachrome was determined by monitoring the absorbance at 475 nm at room temperature. Ascorbic acid was used as standard. The % of inhibition was calculated applying the equation 1 for all mesoionic compounds:

$$\text{Inhibition } \% = \frac{[(B_{30} - B_0) - (A_{30} - A_0)]}{(B_{30} - B_0)} x\ 100 \quad (1)$$

where B_0 and B_{30} are the absorbance values of the control sample at zero time and after 30 min of reaction, respectively. A_0 and A_{30} are the absorbance of the test samples at zero time and after 30 min of reaction, respectively. In the equation 1, the interference of possible absorbance of the organic compounds was subtracted.

In order to calculate the IC_{50} for **PMI-5 and PMI-6** (the most promising tyrosinase inhibitors) the increase in absorption at 475 nm was determined for different inhibitor concentrations. The IC_{50} value was calculated from the equation generated by polinomial fit of the experimental data (Origin software, ANOVA statistical function).

The inhibitory mechanism for **PMI-5** on mushroom tyrosinase for oxidation of L-DOPA was determined from Lineweaver-Burk double reciprocal plots. The Lineweaver-Burk plot is a widely method used to determine important terms in enzyme kinetics, such as K_m, V_{max} and K_i. In this analysis was used the same metodology for the IC_{50} determination, but with different concentrations of L-DOPA (33; 66; 100; 200; 333; 466 and 666 μmol mL^{-1}) as substrate and different concentrations of **PMI-5** (0; 330; 460 and 660 μmol mL^{-1}). After incubation of 30 min at 310 K, the absorbance was measured at 475 nm. Dopachrome production was analyzed in absence and presence of the inhibitors, in the same conditions of the inhibitory test, but the increase in absorption at 475 nm was determined from 0 to 60 min, at 10 min intervals.

2.4. HSA binding studies

Fluorescence and UV-Vis spectra were measured on a Jasco J-815 fluorimeter using a quartz cell (1 cm optical path) and employing a thermostatic cuvette holder Jasco PFD-425S15F. The circular dichroism spectra were measured in a spectropolarimeter Jasco J-815 and employing the same thermostatic cuvette holder as described above. All spectra were recorded with appropriate background corrections.

To a 3.0 mL solution containing an appropriate concentration of HSA ($1.00x10^{-5}$ mol L^{-1}),

successive aliquots from a stock solution of the corresponding mesoionic compounds, *i. e* **PMI-5** and **PMI-6** ($1.00x10^{-3}$ mol L^{-1}) were added, leading to final concentrations of 0.17; 0.33; 0.50; 0.66; 0.83; 0.99; 1.15 and $1.32x10^{-6}$ mol L^{-1}. The addition was done manually by using a micro syringe. The fluorescence spectra were measured in the 290-450 nm range, at 296 K, 303 K and 310 K, with excitation wavelength at 280 nm. The UV-Vis spectra for solutions of **PMI-5** and **PMI-6** ($1.00x10^{-5}$ mol L^{-1}, in methanol) were measured in the 200-450 nm range at 310 K. In order to compensate for the inner filter effect, fluorescence intensity values were corrected for the absorption of each studied mesoionic derivative at the excitation and emission wavelength using equation 2 [26]:

$$F_{cor} = F_{obs} 10^{[(A_{ex}+A_{em})/2]} \quad (2)$$

where F_{cor} and F_{obs} are the corrected and observed fluorescence intensity values, respectively; A_{ex} and A_{em} represent the experimental absorbance values at the excitation wavelength (280 nm) (ε=14942 mol $L^{-1}cm^{-1}$ for **PMI-5** and ε=16966 mol $L^{-1}cm^{-1}$ for **PMI-6**) and emission wavelength (340 nm; ε=10454 mol $L^{-1}cm^{-1}$ for **PMI-5** and ε=8363 mol $L^{-1}cm^{-1}$ for **PMI-6**), respectively.

Circular dichroism spectra were recorded in the 200-260 nm range, at 310 K, for free serum albumin ($1.00x10^{-6}$ mol L^{-1}) and for serum albumin with the highest concentration of **PMI-5** and **PMI-6** ($2.22x10^{-6}$ mol L^{-1}) used in the fluorescence study.

2.5. Molecular modeling

The crystallographic structures of tyrosinase from the mushroom *Agaricus bisporus* and of HSA were obtained from the Protein Data Bank (PDB) with access codes 2Y9X [27] and 1N5U [28], respectively. The mesoionic compounds' structures were built and energy-minimized with the Spartan'14 program (*Wavefunction, Inc.*) at the Density Functional Theory (DFT) level with the Becke-3-Lee Yang Parr (B3LYP) functional, using the 6-31G* basis set [29].

Molecular docking for both protein structures was performed with the GOLD 5.2 program

(CCDC). Hydrogen atoms were added to the protein according to the ionization and tautomeric states inferred by the program [30]. The tyrosinase crystallographic structure is composed by four chains (A, B, C and D) and each chain contains a dicopper center responsible for the tyrosinase activity [27]. In order to propose a molecular explanation for the experimental tyrosinase inhibition data, a 10 Å radius-spherical domain around the dicopper center in the chain D was defined for the molecular docking calculations with the ligands (**PMI-1**,**2**,**3**,**4**,**5** and **6**). Chain D was defined for the molecular docking studies due the best results obtained by the redocking studies with the cocrystallized ligand in the 2Y9X structure, tropolone. As the studied mesoionic compounds presented noncompetitive inhibition (see Results and Discussion section), firstly a tyrosinase:L-DOPA complex was obtained by selecting the corresponding best pose of a molecular docking run of the substrate inside the enzyme implemented with GOLD 5.2. This complex was then used for a second molecular docking run with the **PMI-1-6** ligands. On the other hand, from the fluorescence quenching studies and site-specific drug displacements (see Results and Discussion section), the main HSA cavity for **PMI-5** and **PMI-6** is Sudlow's site I (subdomain IIA), where the Trp-214 residue can be found [31]. In order to identify the main amino acid residues that contribute to the association of **PMI-5** and **PMI-6** with HSA, a 10 Å radius-spherical domain around the tryptophan residue was defined and then molecular docking calculations with both ligands were carried out.

The score of each pose identified is calculated as the negative of the sum of a series of energy terms involved in the protein-ligand interaction process, so that the more positive the score, the better is the interaction. The number of genetic operations (crossover, migration, mutation) in each docking run used in the searching procedure was set to 100,000. The program optimizes hydrogen-bond geometries by rotating all hydroxyl and amino groups of the amino acid side chains. The scoring function used to perform the tyrosinase study was *GoldScore*, the best scoring function identified in the tropolone redocking study. For the HSA docking studies, *ChemPLP* was used, which is the default function of the GOLD 5.2 program [32]. The figures of the docking poses with the largest docking score value were generated with the PyMOL Delano Scientific LLC program

[33].

3. Results and Discussion

3.1. Synthesis

The mesoionic compounds 5-(3,4-methylenedioxy-6-*R*')-1,3,4-thiadiazolium-2-(4-*R*-phenyl)amine chlorides derived from 6-substituted piperonal, where *R'* = *R* = H (**PMI-1**), *R'* = NO_2, *R* = H (**PMI-2**), *R'* = Br, *R* = H (**PMI-3**), *R'* = H, *R* = NO_2 (**PMI-4**), *R'* = H, *R* = Cl (**PMI-5**) and *R'* = H, *R* = Br (**PMI-6**) were sinthesized by microwave assisted irradiation. Of these, **PMI-3**, **PMI-4**, **PMI-5** and **PMI-6** are new compounds. The convergent strategy [18] involved the reaction of the appropriate 3,4-methylenedioxy-6-*R*'-benzaldehyde[23] and N_1-*R*-phenyl-N_4-thiosemicarbazide [24] in the presence of $SOCl_2$ as a Lewis acid catalyst (Scheme 1). Both, the substituted piperonal aldehydes and thiosemicarbazides were also prepared in this work [23,24]. The reaction mixture was irradiated in a microwave oven for 5 min at 100 kW. The products were obtained as fine crystals in high-purity and satisfactory yields, 60 to 95%, after a short irradiation time.

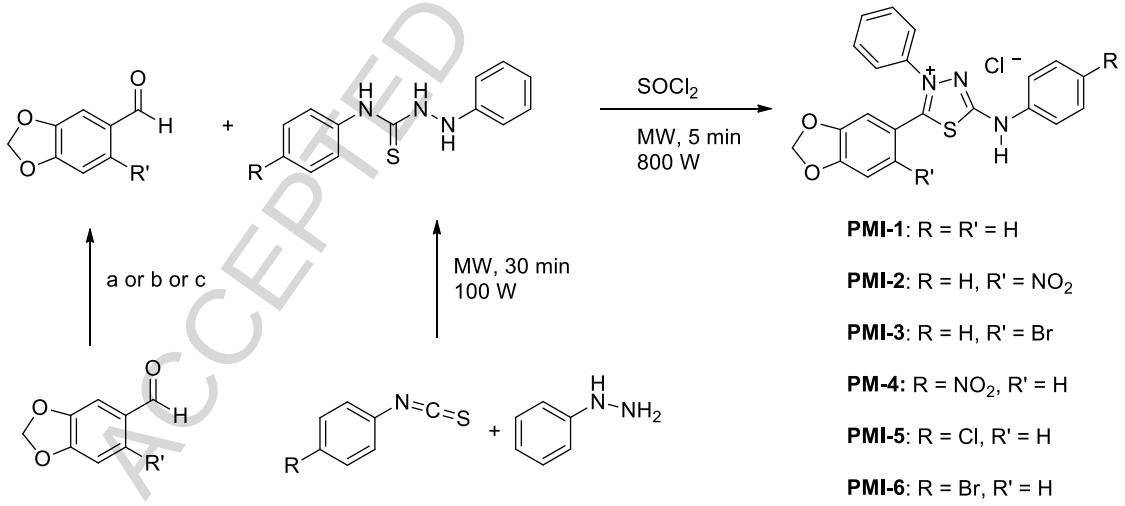

Scheme 1. Reagents and conditions: (a) HNO_3, rt, 30 min; (b) bromine, methanol, acetic acid drops, rt until complete comsumption of piperonal, $NaHSO_4$ (1 $molL^{-1}$).

The synthezised compounds were fully characterized by IR, ^1H and ^{13}C NMR. The ^1H and ^{13}C chemical shifts were assigned based on reported data to other 1,3,4-thiadiazolium-2-phenylamine derivatives [18,25,34] and were consistent with the structures proposed in this work. The chemical shifts of C2 and C5 in the heterocyclic ring appear at high frequencies compared with signals from

the other carbon atoms. The assigned values of δ 160.3 to 162.2 and δ 162.5 to 166.2 for C2 and C5, respectively, showed the coherent correlation with the electronic effects of the substituents. The remaining aromatic carbons in the rings attached to N4 and N-exocyclic were assigned using previous data from the literature [18,25,34].

3.2. Inhibition of mushroom tyrosinase

In order to make a previous test on the inhibitory potential of the mesoionic compounds on the tyrosinase enzyme a screening test was performed (Table 1). The compounds **PMI-1**, **PMI-2**, **PMI-3**, **PMI-5** and **PMI-6** were tested in concentrations of 66.6 and 666 μmol L^{-1}, with exception of **PMI-4,** which was insoluble in this concentration. Therefore, **PMI-4** was only assayed in a 10 fold more diluted solution (*ca.* 66.6 μmol L^{-1} – Table 1).

Table 1. % Inhibition of tyrosinase by mesoionic compounds (66.6 and 666 μmol L^{-1}) in the presence of the substrate L-DOPA.

Compound	Substituent		% Inhibition	% Inhibition
	R	R'	66.6 μM	666 μM
PMI-1	H	H	10	23
PMI-2	H	NO_2	2.0	29
PMI-3	H	Br	1.0	22
PMI-4	NO_2	H	4.0	-
PMI-5	Cl	H	35	89
PMI-6	Br	H	10	79

For the two best tyrosinase inhibitors, **PMI-5** and **PMI-6**, we determined IC_{50} values, which were 124 μmol L^{-1} and 358 μmol L^{-1}, respectively. **PMI-5** showed the most promising tyrosinase inhibition result (Figure S19 in supplementary information) and proved to be a highly effective inhibitor of mushroom tyrosinase, being more efficient than ascorbic acid, the reference inhibitor [35] (in this work, IC_{50} = 260 μmol L^{-1}).

The enzymatic inhibition mechanism was also investigated for the mesoionic compound **PMI-5** by performing a kinetic study in the presence of tyrosinase with different concentrations of the substrate L-DOPA. The corresponding Lineweaver-Burk and Hanes-Woolf plots are depicted in Figures 2A and 2B, respectively.

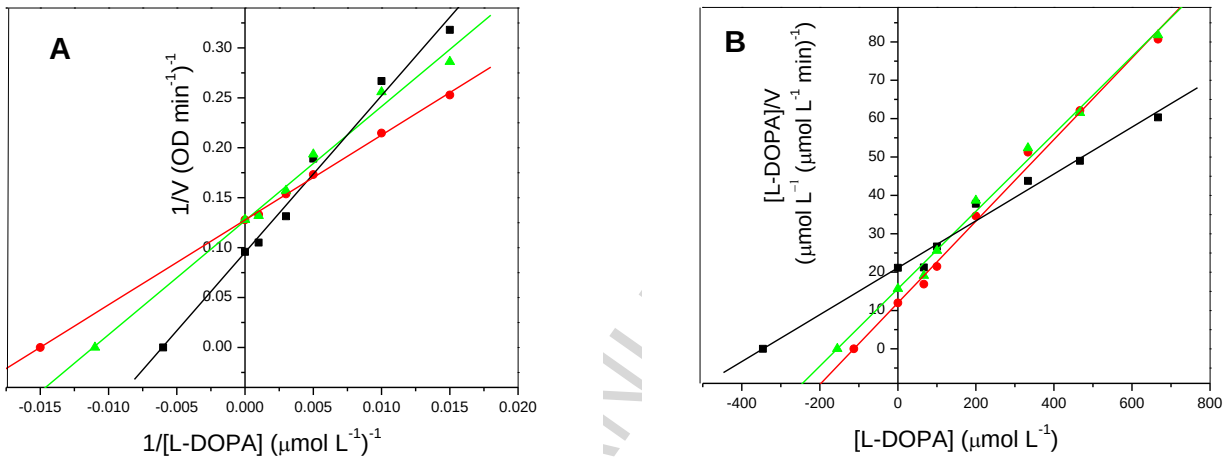

Figure 2. (A) Lineweaver-Burk plot and (B) Hanes-Woolf plot for tyrosinase inhibition, in the absence (control ■) or in the presence of **PMI-5** (♦ 466 μmolL^{-1} and ▲ 333 μmolL^{-1}) with L-DOPA as substrate.

The Lineweaver-Burk plot shows that **PMI-5** acted apparently as a noncompetitive inhibitor, and clearly not as a competitive inhibitor, because the values of K_m and V_m decreased in the presence of inhibitor. A way to distinguish between competitive and noncompetitive inhibitors is employing the Hanes-Woolf plot [36]. In this plot a competitive inhibition exhibits parallel lines, whereas there is an intersection between the lines in the noncompetitive mechanism. In addition, the values of K_m and V_m obtained in Hanes-Woolf plot confirmed the involvement of an noncompetitive mechanism (Table 2). In the noncompetitive mechanism the inhibitor binds reversibly to the complex formed between the enzyme and the substrate (ES complex) and does not bind to the free enzyme.

Table 2. Kinetic parameters obtained from the Lineweaver-Burk and Hanes-Woolf plots for **PMI-5** in the catalytic oxidation of L-Dopa by tyrosinase.

Kinetic parameters		Inhibitor concentration		
		without inhibitor	466 $\mu molL^{-1}$	333 $\mu molL^{-1}$
Lineweaver-Burk	K_m ($\mu molL^{-1}$)	166.6	66.6	90.9
	V_m ($\mu molL^{-1}$ min^{-1})	10.4	7.8	7.8
Hanes-Woolf	K_m ($\mu molL^{-1}$)	345.8	112.6	155.2
	V_m ($\mu molL^{-1}$ min^{-1})	16.4	9.4	9.9

The *in vitro* method to evaluate the inhibitory effect of organic compounds on tyrosinase has a standart time of 30 min [36]. After this time, the inhibition power of the test sample may decrease or remain constant, conferring a stable inhibition mechanism. Based on this, the kinetics of the L-DOPA oxidation by tyrosinase in the absence and presence of the **PMI-5** was evaluated (Figure S20 in supplementary information). The result showed that the concentration of dopachrome produced during the oxidative process was lower in the presence of inhibitor, therefore decreasing the inhibition power, which confirms the noncompetitive mechanism.

3.3. Molecular docking studies for the interaction between tyrosinase and the mesoionic compounds under study

As the experimental tyrosinase assay results showed that the mesoionics compounds under study present a noncompetitive inhibitory mechanism, the potential inhibitors bind reversibly to the complex formed between the enzyme and the substrate L-DOPA (ES complex) and does not to the free enzyme. Based on these experimental informations, a molecular docking study was carried out in order to offer a molecular level explanation on the tyrosinase inhibition by the mesoionic compounds **PMI 1-6**. Figure 3A depicts the best docking pose for all mesoionic compounds in the

presence of L-DOPA. As expected by the presence of the substrate molecule, the potential electron donor piperonal and 1,3,4-thiadiazolium groups present in the ligand structures are not near enough to coordinate with the dicopper center, suggesting that the tyrosinase inhibition by **PMI 1-6** is not related with the Cu^{2+} coordination ability. In fact, is one of the hydroxyl groups from L-DOPA that is near enough to coordinate with the dicopper center, with a distance of 2.30 Å. The molecular surface of tyrosinase (Figure 3A) suggests that L-DOPA is buried inside the enzyme's active site, and **PMI 1-6** are able to interact with L-DOPA, but they are not totally buried inside the protein active site.

The molecular docking results also suggest that the ligands **PMI-5** and **PMI-6,** which showed better experimental inhibition percentage than **PMI-1**, **PMI-2**, **PMI-3**, **PMI-4**, adopt very similar poses inside the protein active site. Despite, molecular docking results also suggest that **PMI-4** (assayed in a 10 fold more diluted solution) could also interacts similar than **PMI-5** and **PMI-6**. The other mesoionic compounds are accomodated diferently inside the protein cavity, resulting in different interactions between the ligands and the amino acid residues present inside the active site. The different interaction pattern presented by **PMI-5** and **PMI-6** in comparison with the remaining mesoionic compounds may be at least in part related to the observed differences in the tyrosinase inhibition activities of these compounds.

Figure 3B presents the superposition of the best docking poses for **PMI-5** and **PMI-6** inside the tyrosinase:L-DOPA active site, showing the main amino acid residues of the enzyme that interact with these two ligands. The Phe-263 residue is interacting *via t*-stacking with the aromatic ring of the piperonal group with a distance of 2.70 Å and the apolar amino acid residue Val-247 residue is interacting *via* hydrophobic interactions with the same aromatic ring, within distance of 2.60 Å. There is a hydrogen bond between the peptidic NH hydrogen of the Val-282 residue and the exociclic nitrogen of the ligand, with a distance of 2.30 and 2.50 Å, for **PMI-5** and **PMI-6**, respectively. Beside these interactions, **PMI-5** and **PMI-6** are able to interact with the aromatic ring

of the substrate L-DOPA *via t*-stacking, within distance of 2.50 Å.

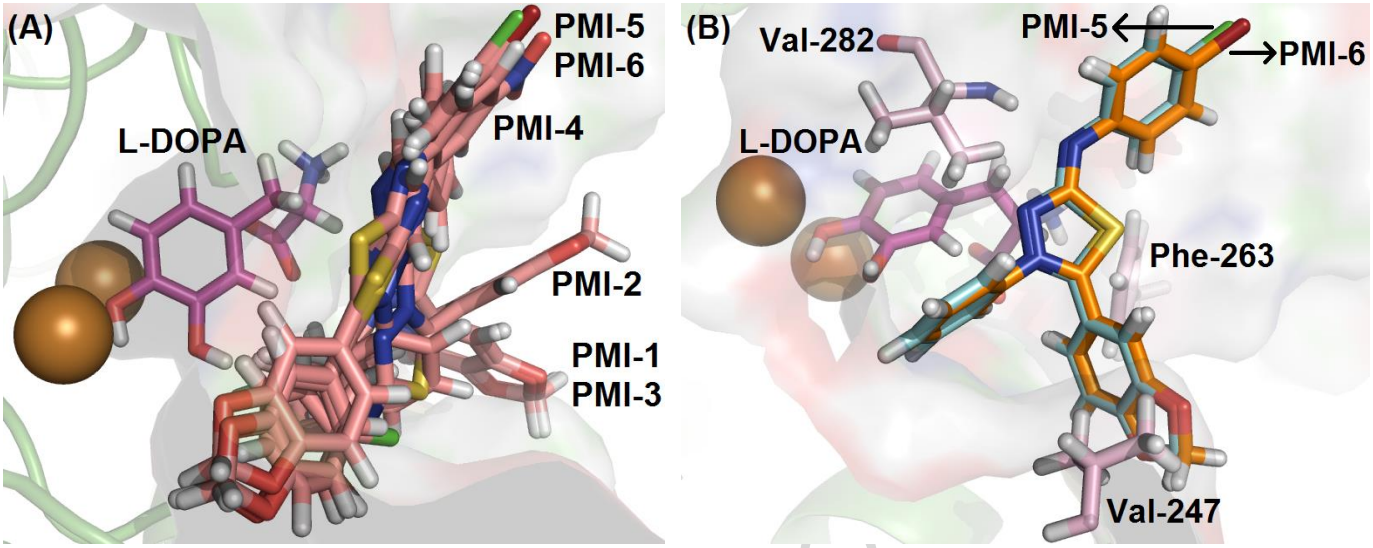

Figure 3. (A) Molecular surface of tyrosinase and its interaction with the mesoionic compounds **PMI-1-6** in the presence of L-DOPA. (B) Superposition of the best docking poses for the interaction of tyrosinase with **PMI-5** and **PMI-6** in the presence of L-DOPA (*GoldScore* function). Tyrosinase is in cartoon representation; L-DOPA, selected amino acid residues and ligands in stick representation are in pink, light pink, and beige, respectively. In the Fig. 3B, **PMI-5** and **PMI-6** are represented in cyan and orange, respectively. Copper atoms are represented as spheres in brown. Element colors: hydrogen: white; oxygen: red; nitrogen: dark blue; bromine: brownish red and chloro: green.

3.4. HSA binding studies – Fluorescence Quenching Analysis

Fluorescence quenching can be used as a technique to measure the binding affinity between macromolecules and ligands acting as quenchers. Quenching of tryptophan (Trp) fluorescence is widely used as a tool to monitor changes in protein structure and to make inferences regarding local structure and dynamics [37]. There is just one tryptophan residue (Trp-214) in the HSA structure, which is located in subdomain IIA, buried inside the protein structure [38]. As can be seen in Figure 4, the fluorescence spectrum of HSA presents a strong emission with maximum at 340 nm (λ_{exc} = 280 nm). After successive additions to the HSA solution of the two mesoionic compounds that showed the highest inhibition % for tyrosinase, *i. e* **PMI-5** and **PMI-6** (see above), the fluorescence emission resulting from the Trp-214 residue showed a clear decrease, indicating that the likely location of the quencher molecule within the protein cavity must be close to the tryptophan residue [39]. The absence of considerable changes in the position of the maximum

emission of HSA is a clear evidence that the presence of **PMI-5** or **PMI-6** does not exert a great influence on the polarity of the cavity microenvironment around the Trp residue [38].

A variety of molecular interactions can result in two possible quenching mechanism of a fluorescent species, *i. e* dynamic or static. These interactions include ground-state complex formation, collisional quenching, excited state reactions, molecular rearrangement and energy transfer [40]. In general, Stern-Volmer analysis (equations 3A and *inset* in the Figure 4), and the well known relationship between k_q and K_{sv} (equation 3B) are useful in the estimation of the accessibility of the quencher molecule to the tryptophan residue in proteins as well as in the understanding of the mechanism involved in the quenching process [37]:

$$\text{(A)} \quad \frac{F_0}{F} = 1 + k_q \tau_0 [Q] = 1 + K_{SV}[Q] \qquad \text{(B)} \quad k_q = \frac{K_{SV}}{\tau_0} \tag{3}$$

where, F_0 and F are the fluorescence intensities for HSA in the absence and in the presence of **PMI-5** or **PMI-6**, respectively; K_{sv} is the Stern-Volmer quenching constant; k_q is the bimolecular quenching rate constant of the HSA fluorescence, [Q] is the ligand concentration and τ_o is the HSA lifetime in the absence of the quencher (10^{-8} s) [38].

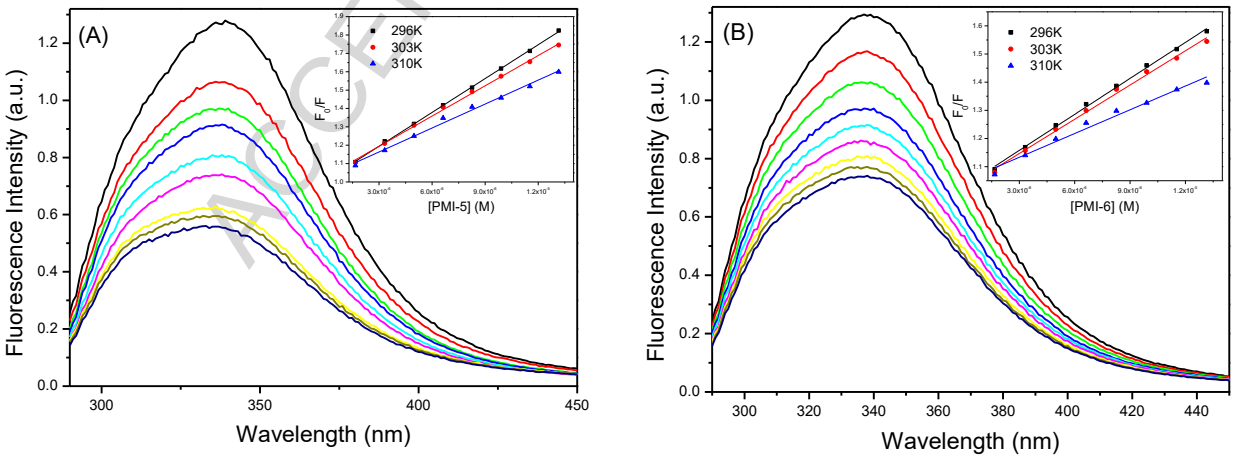

Figure 4. Fluorescence emission spectra forfree HSA and its fluorescence quenching by addition of succesive aliquots of **PMI-5** (A) and **PMI-6** (B). HSA prepared in a PBS buffer solution (pH 7.4). [HSA] = $1.00\text{x}10^{-5}$ mol L^{-1}, [**PMI-5**] = [**PMI-6**] = 0.17; 0.33; 0.50; 0.66; 0.83; 0.99; 1.15 and $1.32\text{x}10^{-6}$ mol L^{-1}, T = 310 K, λ_{exc} = 280 nm. *Inset*: Stern-Volmer plot for the fluorescence

quenching of HSA by **PMI-5** (A) and **PMI-6** (B) at 296 K, 303 K and 310 K.

Table 3 shows the K_{SV} and k_q values obtained from the fluorescence quenching experiments involving HSA:**PMI-5** and HSA:**PMI-6**. Since the bimolecular quenching rate constants obtained ($k_q \approx 10^{12}$ M^{-1} s^{-1}, Table 3) are three orders of magnitude larger than the diffusion rate constant (k_{diff} $\approx$ 5.00x10^9 M^{-1} s^{-1} in water, at 298 K) [41] and the K_{SV} values decrease with the temperature increasing, the probable mechanism of fluorescence quenching is static [42]. Static quenching is due to the formation of an association in the ground-state between the fluorophore (albumin) and the quencher (**PMI-5** or **PMI-6**) [43].

To obtain information about the binding capacity in the interaction HSA:**PMI-5** and HSA:**PMI-6**, the modified Stern-Volmer binding constant (K_a) was calculated employing the modified Stern-Volmer equation (equation 4) according to Figure 5**:**

$$\frac{F_0}{F_0 - F} = \frac{1}{fK_a[Q]} + \frac{1}{f} \qquad (4)$$

where, F_o and F are the fluorescence intensities of HSA without and with the ligand at 340 nm, respectively; K_a is the modified Stern-Volmer binding constant; f is the fraction of the initial fluorescence that is accessible to the quencher and [Q] is the ligand concentration.

The K_a values for the association HSA:**PMI-5** and HSA:**PMI-6** are in the range of 10^4 M^{-1}, showing a moderate interaction between the ligands and HSA [44,45]. From the pharmacological point of view, if drugs are metabolized and excreted from the body too fast because of low protein binding they will be not able to provide their therapeutic effect. On the other hand, if drugs bind too strongly to protein and are metabolized and excreted too slowly, the *in vivo* half-life of these drugs can increase excessively, which may lead to undesired side effects. Therefore, a moderate binding constant to serum albumin is expected for a possible drug candidate [46]. The decrease of K_a values

with the increasing of temperature is in total agreement with the proposed static fluorescence quenching mechanism discussed above [43].

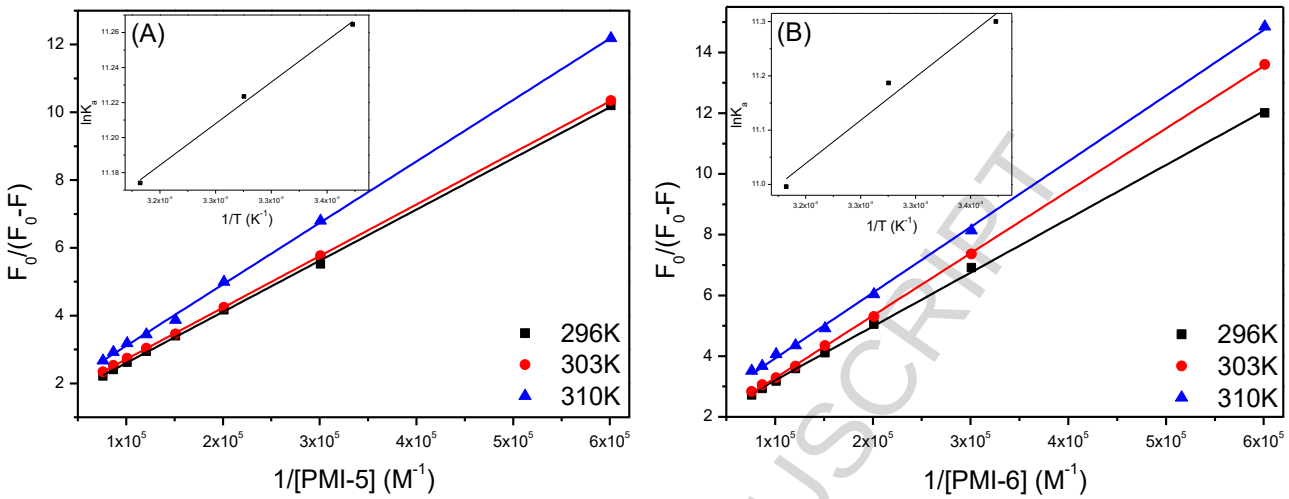

Figure 5. Modified Stern-Volmer plot for fluorescence quenching of HSA upon binding of **PMI-5** (A) and **PMI-6** (B) at 296 K, 303 K and 310 K. *Inset*: Van't Hoff plot of K_a values from modified Stern-Volmer by each ligand at 296 K, 303 K and 310 K. [HSA] = $1.00x10^{-5}$ $molL^{-1}$ and [**PMI-5**] = [**PMI-6**] = 0.17; 0.33; 0.50; 0.66; 0.83; 0.99; 1.15 and $1.32x10^{-6}$ $molL^{-1}$

The interaction forces between endogenous and exogenous agents with proteins (van der Waals and electrostatic forces - including hydrogen bond and hydrophobic effects) can be related to the thermodynamic parameters ΔG°, ΔH° and ΔS°. In this sense, if ΔH°<0 and ΔS°>0 there is an indication that the main force operating is typically through electrostatic effect and hydrophobic interactions [47].

The thermodynamic parameters ΔG°, ΔH°, ΔS°, which control the interaction HSA:**PMI-5** and HSA:**PMI-6** were obtained from the *inset* in Figures **5A** and **5B**, respectively, using the van´t Hoff equation (5A) and the Gibbs free energy equation (5B) [42] and are collected in Table 3.

$$\text{(A)} \quad \ln K_a = -\frac{\Delta H^0}{RT} + \frac{\Delta S^0}{R} \qquad \text{(B)} \quad \Delta G^0 = \Delta H^0 - T\Delta S^0 \qquad (5)$$

where, ΔH°, ΔS°, ΔG° are the enthalpy, entropy and Gibbs free energy, respectively; *R* is the gas

constant (R = 8.314x10^{-3} kJ mol^{-1} K^{-1}), T is the temperature (296 K, 303 K and 310 K) and K_a the modified Stern-Volmer binding constant.

Negative values for the Gibbs free energy change (ΔG°<0; Table 3) are in total accord with the spontaneity of the binding process between HSA and **PMI-5** or **PMI-6**. The negative and positive values for enthalpy and entropy change, respectively, are contributing to the spontaneity of the binding process and by consequence the association HSA:**PMI-5** and HSA:**PMI-6** is enthalpically and entropically driven, suggesting hydrophobic and electrostatic interactions as the main binding forces [48,49].

Table 3. Binding constants (K_{SV}, k_q and K_a) and thermodynamic parameters (ΔH°, ΔS° and ΔG°) for the HSA:**PMI-5** and HSA:**PMI-6** complexes at 296 K, 303 K and 310 K.

Ligand	T (K)	K_{sv} x10^4 (molL^{-1})	k_q x10^{12} (molL^{-1}s^{-1})	K_a x10^4 (molL^{-1})	ΔH (kJ mol^{-1})	ΔS (kJ mol^{-1} K^{-1})	ΔG (kJ mol^{-1})
PMI-5	296	(6.14±0.05)	6.14	(7.80±0.05)	-4.93	0.0770	-27.7
	303	(5.49±0.09)	5.49	(7.49±0.05)	-4.93	0.0770	-28.3
	310	(4.35±0.15)	4.35	(7.13±0.06)	-4.93	0.0770	-28.8
PMI-6	296	(4.26±0.08)	4.26	(8.08±0.06)	-16.5	0.0382	-27.8
	303	(4.05±0.10)	4.05	(7.22±0.05)	-16.5	0.0382	-28.1
	310	(2.81±0.16)	2.81	(5.96±0.08)	-16.5	0.0382	-28.3

Obs.: r^2 = 0.9997-0.9918 for all measurements listed above.

*3.5. Energy transfer from HSA to **PMI-5** and **PMI-6***

Fluorescence resonance energy transfer (FRET) is an electrodynamic phenomenon that occurs between a donor molecule in its excited state and an acceptor molecule in the ground state. Non-radiative energy transfer occurs when the electronic excitation energy of a donor chromophore (Tryptophan in HSA) is transferred to an acceptor molecule (halogenated mesoionic compounds) by a dipole-dipole interaction [50]. The efficiency of energy transfer (E) can be given by the equations

6A and 6B [51].

$$\text{(A)} \qquad E = 1 - \frac{F}{F_0} = \frac{R_0^6}{R_0^6 + r^6} \qquad \text{(B)} \qquad r^6 = \frac{R_0^6 . (1 - E)}{E} \qquad (6)$$

where F_0 and F are the donor fluorescence intensities in the absence and in the presence of an acceptor, respectively; r is the distance between acceptor and donor; R_0 is the critical distance for transfer efficiency of 50%, which can be determined by equation 7:

$$R_0^6 = 8.8 x 10^{-25} K^2 n^{-4} \Phi J \qquad (7)$$

where K^2 is the spatial orientation factor of the dipole (K^2 = 2/3 for random orientation in fluid solution), n is the averaged refraction index of the medium (usually resulting in a value of 1.336, which is the average for water containing organic material), [52] Φ is the fluorescence quantum yield of the donor (HSA) in the absence of quencher (Φ = 0.118) [53] and J is the overlap integral between the emission spectrum of the donor and the absorption spectrum of the acceptor. J can be calculated from Figure 8A and 8B and equation 8:

$$J = \frac{\int_0^\infty F(\lambda)\varepsilon(\lambda)\lambda^4 \, d\lambda}{\int_0^\infty F(\lambda) \, d\lambda} = \frac{\sum F(\lambda)\varepsilon(\lambda)\lambda^4 \, \Delta\lambda}{\sum F(\lambda) \, \Delta\lambda} \qquad (8)$$

where $F(\lambda)$ is the normalized fluorescence intensity of the donor at the wavelength λ and $\varepsilon(\lambda)$ is the extinction coefficient of the acceptor at λ.

Figure 6 shows the spectral overlap between the fluorescence emission spectrum of HSA and the absorption spectrum of **PMI-5** and **PMI-6**, indicating that there is a reasonable probability of an energy transfer process from HSA to **PMI-5** and **PMI-6** [54]. The calculated values for the distances between HSA (as donor) and each of the ligands (as acceptors) (r) shown in Table 4 is between 2 and 8 nm, in full agreement with the rule $0.5R_0 < r < 1.5R_0$, confirming the high probability of occurrence of energy transfer between albumin and **PMI-5** or **PMI-6** [53].

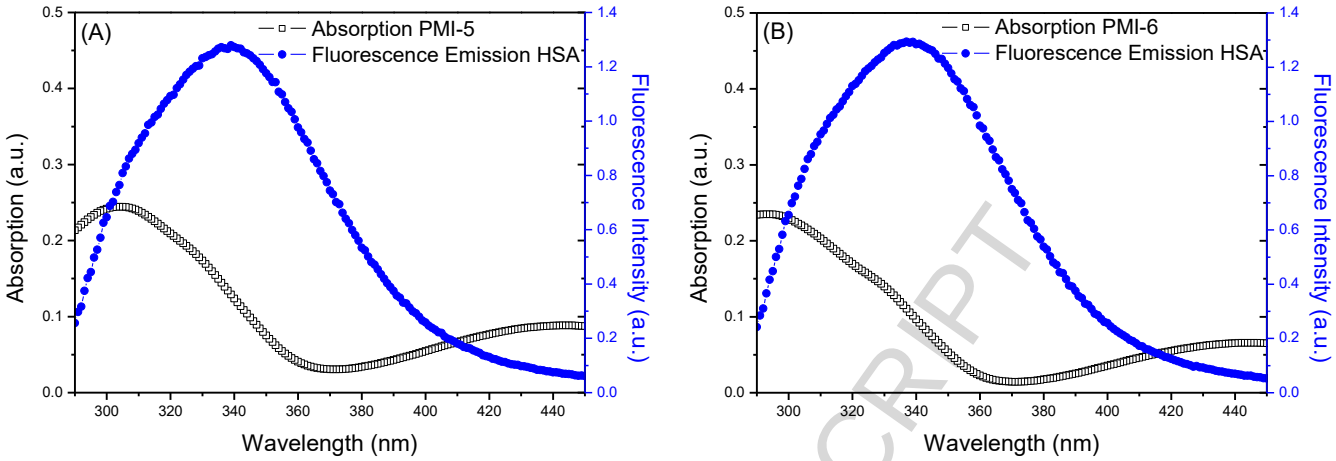

Figure 6. Spectral overlap between the fluorescence emission spectrum of HSA and the absorption spectra of **PMI-5** (A) and **PMI-6** (B), respectively, at 310 K. [HSA] = [**PMI-5**] = [**PMI-6**] = 1.00×10^{-5} molL^{-1} at 310 K.

Table 4. Parameters to estimate the spatial distance between the donor (HSA) and the acceptor (**PMI-5** and **PMI-6**) measured by the FRET theory.

Sample	J (cm^3 molL^{-1})	R_0 (nm)	r (nm)
PMI-5	$1.55\text{x}10^{-14}$	2.64	2.99
PMI-6	$1.20\text{x}10^{-14}$	2.53	2.82

*3.6. Identification of the main binding site on HSA structure for the association with **PMI-5** and **PMI-6***

HSA crystal structure analysis revealed that its main drug binding sites are located in subdomains IIA and IIIA, also known as Sudlow's site I and II, respectively. A large hydrophobic cavity is present in the IIA subdomain whereas a hydrophilic cavity is present in the subdomain IIIA. In order to further identify the main binding site for **PMI-5** and **PMI-6** on the HSA structure,

competitive binding experiments were carried out at 310 K using warfarin and ibuprofen as specific site markers for the Sudlow's site I and II, respectively [31,52,54].

The modified Stern-Volmer binding constant (K_a) values at 310 K for HSA:**PMI-5** and HSA:**PMI-6** binding in the presence of warfarin was reduced by 96.8% ($2.26x10^3$ mol L^{-1}) and 96.1% ($2.30x10^3$ mol L^{-1}), respectively, as determined by using equation 4 (Figure S21 in supplementary information). On the other hand, in the presence of ibuprofen the K_a values for HSA:**PMI-5** and HSA:**PMI-6** binding were reduced by only 18.9% ($5.78x10^4$ mol L^{-1}) and 20.5% ($4.74x10^4$ mol L^{-1}), respectively. As the K_a values in the absence and in the presence of ibuprofen are practically the same, whereas they change significantly in the presence of warfarin, this is a clear evidence that both **PMI-5** and **PMI-6** compete with warfarin for the same binding site in HSA, *i. e* the subdomain IIA, where the Trp-214 residue can be found [49].

*3.7. Perturbation on the HSA secondary structure induced by **PMI-5** and **PMI-6***

To understand the alteration in the protein secondary structure after addition of the mesoionic compounds **PMI-5** and **PMI-6** to its surroundings, Circular Dichroism spectroscopy (CD) was employed due to its sensitive prediction [54]. HSA exhibited two negative bands in the CD spectra: one at 208 nm that corresponds to the highest electronic energy transition (π-π^*) and another at 222 nm that corresponds to the lowest electronic energy transition (n-π^*), both of which are characteristic of the α-helix structure units of the protein [55]. As can be seen in **Figures 7A and 7B,** a decrease in the intensity at 208 nm and 222 nm is clearly observed upon the adition of the maximum concentration of the ligands used in the fluorescence quenching studies . These data indicate a strong change on the secondary structure of HSA [56].

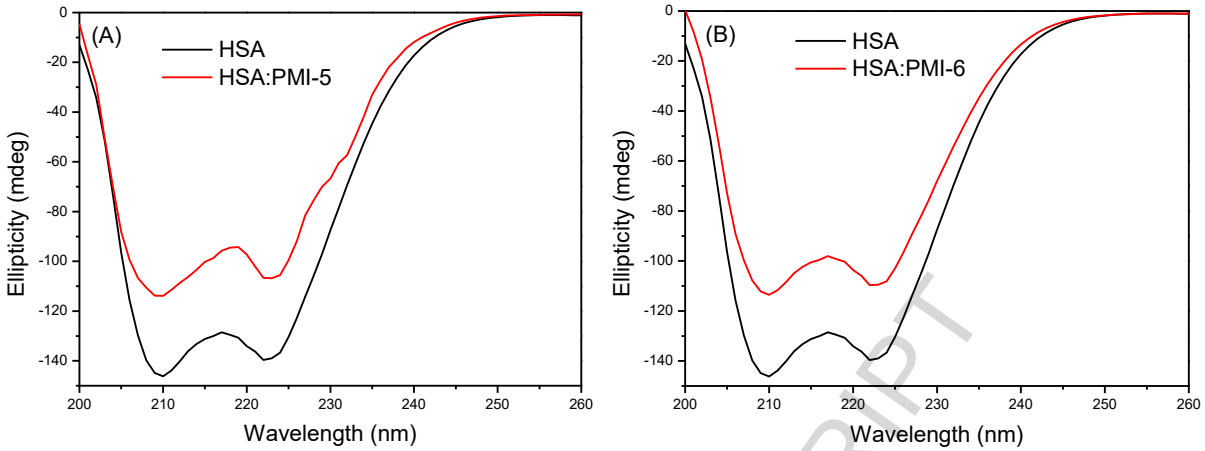

Figure 7. Circular dichroism spectra of HSA in the absence and presence of the mesoionic compounds **PMI-5** (A) and **PMI-6** (B) in a PBS buffer solution (pH=7.4). [HSA] = $1.00x10^{-6}$ $molL^{-1}$ and [**PMI-5**] = [**PMI-6**] = $1.32x10^{-5}$ $molL^{-1}$.

In order to offer a quantitative decrease on the loss of helical structure (α-helix %) due to the ligand binding, firstly the CD results were expressed in terms of significant molar residual ellipticity (MRE) in $deg.cm^2/dmol$, which were calculated according to equation 9:

$$MRE = \frac{\theta}{(10.n.l.C_P)} \tag{9}$$

where, θ is the observed ellipticity (mdeg); *n* is the number of amino acid residues (585 to HSA) [57] *l* is the length of the optical cuvette (1.0 cm) and C_p is the molar concentration of HSA ($1.00x10^{-6}$ mol L^{-1}).

The α-helix % is calculated as contents of either free HSA or complexed with each ligand from the MRE values at 208 nm and 222 nm, using equations 10A and 10B:

$$\text{(A)}\ \alpha\text{-}helix\% = \frac{\left(-MRE_{208} - 4000\right)}{(33000 - 4000)}\ x\ 100 \qquad \text{(B)}\ \alpha\text{-}helix\% = \frac{\left(-MRE_{222} - 2340\right)}{30300}\ x\ 100 \tag{10}$$

where, MRE_{208} and MRE_{222} are the significant molar residual ellipticities (deg cm^2 $dmol^{-1}$) at 208 nm and 222 nm, respectively.

The calculated α-helix content of the secondary structure of HSA in the absence of the ligands has its maximum at about 72.3% (at 208 nm) and 70.7% (at 222 nm) at 310K. In presence of the ligand, *i. e* **PMI-5** or **PMI-6** ($1.32x10^{-5}$ mol L^{-1}), the calculated α-helix content was about 53.3% and 53.1% at 208 nm for HSA:**PMI-5** and HSA:**PMI-6**, respectively. On the other hand, under the very same conditions the calculated α-helix content was 52.4% and 54.1% at 222 nm for HSA:**PMI-5** and HSA:**PMI-6**, respectively. These results indicate that the ligands perturbate significantly the secondary structure of albumin, possibly destroying the hydrogen bonding networks of the amino acid residues of the main polypeptide chain due the high kinetic volume of each ligand and its charged nature [58]. In the literature, interaction between serum albumin and some thiadiazole derivatives, as well as 3-carboxyphenoxathiin, chalcone and some charged surfactants (C_{14}HDAB and C_{14}DHAB) also suggested high perturbation on the secondary structure of the protein, although still remains predominantly α-helix [58,59-61].

*3.8. Molecular docking studies for the interaction between HSA and **PMI-5** or **PMI-6***

From the experimental studies of HSA fluorescence quenching, it is clear that **PMI-5** and **PMI-6** are binding next to the Trp-214 residue and did not show major differences in their binding ability. Studies using molecular docking were performed to analyze the main intermolecular interactions between **PMI-5** and **PMI-6** with the amino acid residues present in the binding site (Sudlow's site I). **Figure 8** shows the superposition of the best poses obtained for the interaction of **PMI-5** and **PMI-6** with HSA. The molecular docking results suggest that both molecules are able to interact with hydrophobic and hydrophilic amino acid residues. One of the oxygen atoms of the piperonal group of both ligands behaves as an acceptor for a weak hydrogen bond from the Arg-221 residue, with distances of 3.61 Å and 3.80 Å, for **PMI-5** and **PMI-6**, respectively; while the protonated amino group of Lys-198 residue is interacting by a hydrogen bond with one of the nitrogen atoms present in the 1,3,4-thiadiazolium ring of the ligands with a distance of 2.67 Å, for both ligands. On the other hand, the intrinsic fluorophore of albumin, the Trp-214 residue,

participates of *t*-stacking interactions with the aromatic ring of each ligand with distances of 2.52 Å and 2.65 Å, for **PMI-5** and **PMI-6**, respectively. Finally, the molecular docking results also suggest that ligands can have hydrophobic interactions with the side chains of the amino acids Leu-197, and Leu-480 residues.

Overall, for HSA the molecular docking results suggest that both ligands are able to be accommodated in the Trp-214 residue-containing site, interacting with the same amino acid residues, with only small differences on the interaction distances, which is in accordance with their similar experimental binding constants.

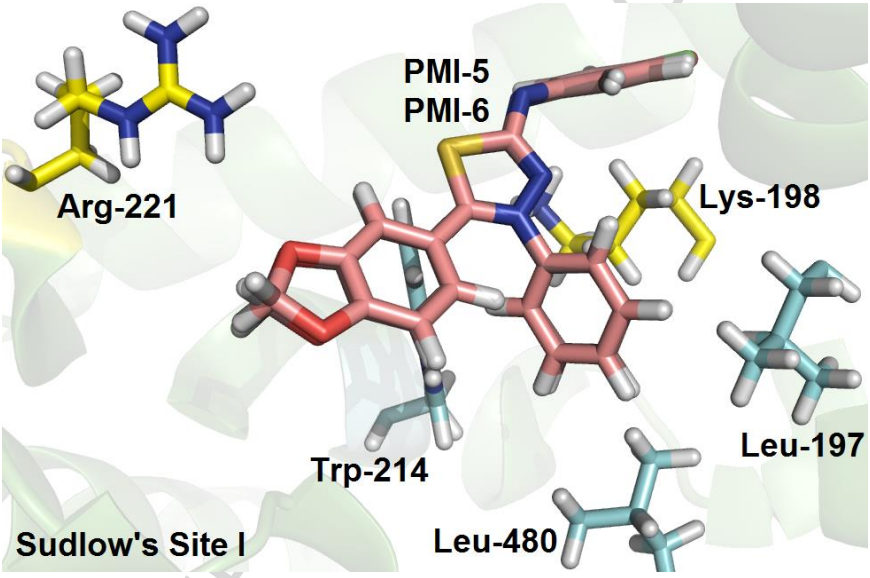

Figure 8. Superposition of the best docking pose for the interaction between HSA:**PMI-5** and HSA:**PMI-6** (*ChemPLP* function). HSA structure is in cartoon representation; **PMI-5**, **PMI-6** and selected hydrophobic and hydrophilic amino acid residues in stick representation are in brown, beige, cyan and yellow, respectively. Element colors: hydrogen: white; oxygen: red; nitrogen: dark blue; bromine: carnelian and chloro: green.

4. Conclusions

A novel series of 1,3,4-thiadiazolium-2-phenylamine mesoionic compounds was synthesized by microwave assisted irradiation. The two mesoionic compounds that showed the highest tyrosinase inhibition were **PMI-5** and **PMI-6**. Between them, **PMI-5** is the most promising tyrosinase inhibitor through a noncompetitive inhibitory mechanism and a IC_{50} = 124

μmol L^{-1}, being more efficient than the commercial inhibitor ascorbic acid (IC_{50} at 260 μmol L^{-1}). These results were supported by molecular docking studies of the compounds with the tyrosinase:L-DOPA complex. The K_{SV} and k_q values obtained from Stern-Volmer plots indicated that the intrinsic fluorescence quenching of HSA by **PMI-5** and **PMI-6** occurs through a static mechanism. Therefore, an association HSA:**PMI-5** and HSA:**PMI-6** in the ground state can be expected. Energy transfer from HSA to either **PMI-5** or **PMI-6** can occur with high probability. The modified Stern-Volmer binding constant values ($K_a \approx 10^4$ mol L^{-1}) results indicated that the association HSA:**PMI-5** and HSA:**PMI-6** is moderate. Besides, CD studies show that upon HSA:**PMI-5** and HSA:**PMI-6** association can significantly perturb the secondary structure of albumin, possibly destroying the hydrogen bonding networks of the amino acid residues of the main polypeptide chain. Thermodynamic parameters indicated that the association HSA:**PMI-5** and HSA:**PMI-6** is spontaneous ($\Delta G° < 0$) and both are enthalpically and entropically driven. The molecular docking results suggest that **PMI-5** and **PMI-6** are able to be accommodated in the Trp-214-containing binding site of HSA, interacting with the same amino acid residues, with only small differences on the distances between them and the HSA residues**.**

Conflict of interest

Authors declare no conflict of interest.

Acknowledgements

This research was supported by the Brazilian funding agencies: Coordenação de Aperfeiçoamento de Pessoal de Nível Superior (CAPES), Conselho Nacional de Desenvolvimento Científico e Tecnológico (CNPq) and Fundação de Amparo à Pesquisa do Estado do Rio de Janeiro (FAPERJ).

Author Contributions

N.D.L. and D.S.-P. synthesized the mesoionic derivatives, M.C.C.O. conducted tyrosinase assays, O.A.C. conducted HSA spectroscopic experiments and molecular docking experiments for HSA and tyrosinase, C.M.R.S. professor responsible for molecular docking analysis, J.C.N.-F. professor responsible for spectroscopic analysis, A.E. professor responsible for synthesis.

References

1. K.G. Strothkemp, R.L. Jolley, H.S. Mason, Quaternary structure of mushroom tyrosinase, Biochem. Biophys. 70 (1976) 519-524.
2. M. Brenner, V.J. Hearing, The protective role of melanin against UV damage in human skin, Photochem. Photobiol. 84 (2008) 539-549.
3. Y. Xu, A.H. Stokes, S.C. Freeman, B.A. Kumer, B.A. Vogt, K.E. Vrana, Tyrosinase mRNA is expressed in human substantia nigra, Mol. Brain Res. 45 (1997) 159-162.
4. S. Parvez, M. Kang, H.S. Chung, H. Bae, Naturally occurring tyrosinase inhibitors: mechanism and applications in skin health, cosmetics and agriculture industries, Phytother. Res. 21 (2007) 805-816.
5. P. Ruzza, P.A. Serra, D. Fabbri, M.A. Dettori, G. Rocchitta, G. Delogu, Hydroxylated biphenyls as tyrosinase inhibitor: A spectrophotometric and electrochemical study, Eur. J. Med. Chem. 126 (2017) 1034-1038.
6. M.R. Loizzo, R. Tundis, F. Menichini, Natural and synthetic tyrosinase inhibitors as antibrowning agents: An update, Compr. Rev. Food Sci. Food Saf. 11 (2012) 378-398.
7. J.W. Park, Y.M. Ha, K.M. Moon, S.R. Kim, H.O. Jeong, Y.J. Park, H.J. Lee, J.Y. Park, Y.M. Song, P. Chun, Y. Byun, H.R. Moon, H.Y. Chung, De novo tyrosinase inhibitor: 4-(6,7-dihydro-5H-indeno[5,6-d]thiazol-2-yl)benzene-1,3-diol (MHY1556), Bioorg. Med. Chem. Lett. 23 (2013) 4172-4176.

8. H. Hamidian, R. Tagizadeh, S. Fozooni, V. Abbasalipour, A. Taheri, M. Namjou, Synthesis of novel azo compounds containing 5(4H)-oxazolone ring as potent tyrosinase inhibitors, Bioorg. Med. Chem. 21 (2013) 2088-2092.
9. Z. Zhou, J. Zhuo, S. Yan, L. Ma, Design and synthesis of 3,5-diaryl-4,5-dihydro-1H-pyrazoles as new tyrosinase inhibitors, Bioorg. Med. Chem. 21 (2013) 2156-2162.
10. K.W. Lam, A. Syahida, Z. Ul-Haq, M.B.A. Rahman, N.H. Lajis, Synthesis and biological activity of oxadiazole and triazolothiadiazole derivatives as tyrosinase inhibitors, Bioorg. Med. Chem. 20 (2010) 3755-3759.
11. E.L. Bizetto, G.R. Noleto, A. Echevarria, A.V. Canuto, S.M.S.C. Cadena, Effect of sydnone SYD-1 on certain functions of LPS-stimulated macrophages, Mol. Cell Biochem. 360 (2012) 15-21.
12. Nithinchandra, B. Kalluraya, S. Aamir, A.R. Shabaraya, Regioselective reaction: synthesis, characterization and pharmacological activity of some new Mannich and Schiff bases containing sydnone, Eur. J. Med. Chem. 54 (2012) 597-604.
13. R.O. Paiva, L.F. Kneipp, C.M. Reis, A. Echevarria, Mesoionic compounds with antifungal activity against fusarium verticillioides, BMC Microbiol. 15 (2015) 1-8.
14. V.K. Akbari, P.P. Savaliya, K.C. Patel, Synthesis and antimicrobial activity of 2-substituted-3-((3-(6-nitrobenzo[D]thiazol-2-yl)-4-oxo-3,4-dihydroquinazolin-2-yl)methyl)-1,3,4-thiadiazol-3-ium-5-thiolate, Phosphorus Sulfur Silicon Relat. Elem. 189 (2014) 711-719.
15. R.F. Rodrigues, E.F. Da Silva, A. Echevarria, R. Fajardo-Bonin, V.F. Amaral, L.L. Leon, M.M. Canto-Cavalheiro, A comparative study of mesoionic compounds in Leishmania sp. and toxicity evaluation, Eur. J. Med. Chem. 42 (2007) 1039-1043.
16. R.J. Soares-Bezerra, L.L. Leon, A. Echevarria, C.M. Reis, L. Gomes-Silva, C.G. Agostinho, R.A. Fernandes, M.M. Canto-Cavalheiro, M.S. Genestra, In vitro evaluation of 4-phenyl-5-(4'-X-phenyl)-1,3,4-thiadiazolium-2-phenylaminide chlorides and 3[N-4'-X-phenyl]-1,2,3-

oxadiazolium-5-olate derivatives on nitric oxide synthase and arginase activities of Leishmania amazonensis, Exp. Parasitol. 135 (2013) 50-54.

17. Y. Li, J. Geng, Y. Liu, S. Yu, G. Zhao, Thiadiazole - a promising structure in medicinal chemistry, Chem. Med. Chem. 8 (2013) 27-41.
18. C.M. Reis, J. Echevarria-Lima, A.F. Miranda, A. Echevarria, Improved synthesis of 1,3,4-thiadiazolium-2-phenylamines using microwave and ultrasound irradiation and investigation of their cytotoxic activity, J. Braz. Chem. Soc. 22 (2011) 1505-1510.
19. A.P. Brandt, J.J. Gozzi, A.R.A. Pires, G.R. Martinez, A.V.S. Canuto, A. Echevarria, A. Di Pietro, S.M.S.C. Cadena, Impairment of oxidative phosphorylation increases the toxicity of SYD-1 on hepatocarcinoma cells (HepG2), Chem. Biol. Interact. 256 (2016) 154-160.
20. S.T. Asundaria, C. Pannecouque, E. De Clercq, C.T. Seipuran, K.C. Patel, Synthesis of novel biologically active methylene derivatives of sydnones, Med. Chem. Res. 22 (2013) 5752-5763.
21. M.B. Shahsavani, S. Ahmadi, M.D. Aseman, S.M. Nabavizadeh, M.M. Alavianmehr, R. Yousef, Comparative study on the interaction of two binuclear Pt (II) complexes with human serum albumin: Spectroscopic and docking simulation assessments, J. Photochem. Photobiol. B: Biol. 164 (2016) 323-334.
22. A. Burmudzija, Z. Ratkovic, J. Muskinja, N. Jankovic, B. Rankovic, M. Kosanic, S. Đorđevic, Ferrocenyl based pyrazoline derivatives with vanillic core: synthesis and investigation of their biological properties, RSC Adv. 6 (2016) 91420-91430.
23. J.L.R. Melos, E.C. Torres-Santos, V.S. Faiões, C.N. Del Cistia, C.M.R. Sant'Anna, C.E. Rodrigues-Santos, A. Echevarria, Novel 3,4-methylenedioxyde-6-X-benzaldehyde-thiosemicarbazones: Synthesis and antileishmanial effects against Leishmania amazonensis, Eur. J. Med. Chem. 103 (2015) 409-417.
24. C.M. Reis, D. Sousa-Pereira, A. Echevarria, Microwave-assisted synthesis of new N_1,N_4-substituted thiosemicarbazones, Molecules 16 (2011) 10668-10684.

25. W.S. Ferreira, L. Freire-de-Lima, V.B. Saraiva, F. Alisson-Silva, L.M. Previato, J.O. Previato, A. Echevarria, M.E. Freire-de-Lima, Novel 1,3,4-thiadiazolium-2-phenylamine chlorides derived from natural piperine as trypanocidal agents: Chemical and biological studies, Bioorg. Med. Chem. 16 (2008) 2984-2991.

26. O.A. Chaves, C.S.H. Jesus, P.F. Cruz, C.M.R. Sant'Anna, R.M.M. Brito, C. Serpa, Evaluation by fluorescence, STD-NMR, docking and semi-empirical calculations of the o-NBA photo-acid interaction with BSA, Spectrochimica Acta Part A 169 (2016) 175-181.

27. W.T. Ismaya, H.J. Rozeboom, A. Weijn, J.J. Mes, F. Fusetti, H.J. Wichers, B.W. Dijkstra, Crystal structure of agaricus bisporus mushroom tyrosinase: Identity of the tetramer subunits and interaction with tropolone, Biochemistry. 50 (2011) 5477-5486.

28. M. Wardell, Z. Wang, J.X. Ho, J. Robert, F. Ruker, J. Ruble, D.C. Carter, The atomic structure of human methemalbumin at 1.9 A, Biochem. Biophys. Res. Comm. 291 (2002) 813-819.

29. W.J. Hehre, A Guide to Molecular Mechanics and Quantum Chemical Calculations; Wavefunction, Inc., Irvine, USA, 2003.

30. http://www.ccdc.cam.ac.uk/solutions/csd-discovery/components/gold/ accessed in July 2017.

31. Z. Sun, H. Xu, Y. Cao, F. Wang, W. Mi, Elucidating the interaction of propofol and serum albumin by spectroscopic and docking methods, J. Mol. Liq. 219 (2016) 405-410.

32. O. Korb, T. Stützle, T.E.J. Exner, Empirical scoring functions for advanced protein-ligand docking with PLANTS, Chem. Inf. Model. 49 (2009) 84-96.

33. W.L. DeLano, PyMOL User's Guide; DeLano Scientific LLC, USA, 2002.

34. A.C.S. Santos. A. Echevarria, Electronic effects on ^{13}C-NMR chemical shifts of substituted 1,3,4-thiadiazolium salts, Magn. Reson. Chem. 39 (2001) 182-186.

35. Y.J. Kim, K. Uyama, Tyrosinase inhibitors from natural and synthetic sources: structure, inhibition mechanism and perspective for the future, Cell. Mol. Life Sci. 62 (2005) 1707-1723.

36. I.H. Segel, Cálculos de Bioquímica , Acribia, 2ª Ed., 1982.

37. J.R. Lakowicz, Principles of Fluorescence Spectroscopy, 1st ed.; Springer: New York, NY, USA, 2006.

38. O.A. Chaves, A.P.O. Amorim, L.H.E. Castro, C.M.R. Sant'Anna, M.C.C. de Oliveira, D. Cesarin-Sobrinho, J.C. Netto-Ferreira, A.B.B. Ferreira, Fluorescence and docking studies of the interaction between human serum albumin and pheophytinMolecules 20 (2015) 19526-19539.

39. J. Liu, J.N. Tian, J. Zhang, Z. Hu, X. Chen, Interaction of magnolol with bovine serum albumin: a fluorescence–quenching study, Anal. Bioanal. Chem. 376 (2003) 864-867.

40. N. Jankovic, J. Muskinja, Z. Ratkovic, Z. Bugarci, B. Rankovic, M. Kosanic, S. Stefanovic, Solvent-free synthesis of novel vanillidene derivatives of Meldrum's acid: biological evaluation, DNA and BSA binding study, RSC Adv. 6 (2016) 39452-39459.

41. D. Brune, S. Kim, Predicting protein diffusion coefficients, Biophysics. 90 (1993) 3835-3839.

42. P.L. Gentili, F. Ortica, G. Favaro, Static and dynamic interaction of a naturally occurring photochromic molecule with bovine serum albumin studied by UV-visible absorption and fluorescence spectroscopy, J. Phys. Chem. B 112 (2008) 16793-16801.

43. O.A. Chaves, V.A. da Silva, C.M.R. Sant'Anna, A.B.B. Ferreira, T.A.N. Ribeiro, M.G. de Carvalho, D. Cesarin-Sobrinho, J.C. Netto-Ferreira, Binding studies of lophirone B with bovine serum albumin (BSA): Combination of spectroscopic and molecular docking techniques, J. Mol. Struct. 1128 (2017) 606-611.

44. O.A. Chaves, C.S.H. Jesus, E.S. Henriques, R.M.M. Brito, C. Serpa, In situ ultra-fast heat deposition does not perturb the structure of serum albumin, Photochem. Photobiol. Sci. 15 (2016) 1524-1535.

45. J.N. Tian, J. Liu, Z.D. Hu, X.G. Chen, Interaction of wogonin with bovine serum albumin, Bioorg. Med. Chem. 13 (2005) 4124-4129.

46. L.S. de Barros, O.A. Chaves, E. Schaeffer, C.M.R. Sant'Anna, A.B.B. Ferreira, D. Cesarin-Sobrinho, F.A. da Silva, J.C. Netto-Ferreira, Evaluating the interaction between di-fluorinated chalcones and plasmatic albumin, J. Fluor. Chem. 190 (2016) 81-88.

47. O.A. Chaves, B.A. Soares, M.A.M. Maciel, C.M.R. Sant'Anna, J.C. Netto-Ferreira, D. Cesarin-Sobrinho, A.B.B. Ferreira, A study of the interaction between trans-dehydrocrotonin, a bioactive natural 19-nor-clerodane, and serum albumin, J. Braz. Chem. Soc. 27 (2016) 1858-1865.

48. P.D. Ross, S. Subramanian, Thermodynamics of protein association reactions: forces contributing to stability, Biochemistry 20 (1981) 3096-3102.

49. O.A. Chaves, D. Cesarin-Sobrinho, C.M.R. Sant'Anna, M.G. de Carvalho, L.R. Suzart, F.E.A. Catunda-Junior, J.C. Netto-Ferreira, A.B.B. Ferreira, Probing the interaction between 7-O-β-D-glucopyranosyl-6-(3-methylbut-2-enyl)-5,4-dihydroxyflavonol with bovine serum albumin (BSA), J. Photochem. Photobiol. A Chem. 336 (2017) 32-41.

50. Z. Bai, Y. Liu, P. Zhang, J. Guo, Y. Ma, X. Yun, X. Zhao, R. Zhong, F. Zhang, Fluorescence resonance energy transfer between bovine serum albumin and fluoresceinamine, Luminescence 31 (2016) 688-693.

51. A. Safarnejad, M. Shaghaghi, G. Dehghan, S. Soltani, Binding of carvedilol to serum albumins investigated by multi-spectroscopic and molecular modeling methods, J. Lumin. 176 (2016) 149-158.

52. O.A. Chaves, C.H.C.S. de Oliveira, R.C. Ferreira, R.P. Pereira, J.L.R. de Melos, C.E. Rodrigues-Santos, A. Echevarria, D. Cesarin-Sobrinho, Investigation of interaction between human plasmatic albumin and potential fluorinated anti-trypanosomal drugs, J. Fluor. Chem. 199 (2017) 103-112.

53. S.N. Khana, B. Islama, R. Yennamalli, A. Sultana, N. Subbarao, A.U. Khan, Interaction of mitoxantrone with human serum albumin: Spectroscopic and molecular modeling studies, Eur. J. Pharm. Sci. 35 (2008) 371-382.

54. Y.J. Hu, Y. Liu, R.M. Zhao, J.X. Dong, S.S. Qu, Spectroscopic studies on the interaction between methylene blue and bovine serum albumin, J. Photochem. Photobiol. A: Chem. 179 (2006) 324-329.

55. M.A. Khan, S. Muzammil, J. Musarrat, Differential binding of tetracyclines with serum albumin and induced structural alterations in drug-bound protein, Int. J. Biol. Macromol. 30 (2002) 243-249.

56. Y. Qian, X. Zhou, J. Chen, Y. Zhang, Binding of bezafibrate to human serum albumin: insight into the non-covalent interaction of an emerging contaminant with biomacromolecules, Molecules. 17 (2012) 6821-6831.

57. I. Matei, M. Hillebrand, Interaction of kaempferol with human serum albumin: a fluorescence and circular dichroism study, J. Pharm. Biomed. Anal. 51 (2010) 768-773.

58. K.M. Naik, S.T. Nandibewoor, Spectroscopic studies on the interaction between chalcone and bovine serum albumin, J. Lumin. 143 (2013) 484-491.

59. S. Karthikeyan, G. Bharanidharan, K.A. Mani, N. Srinivasan, M. Kesherwani, D. Velmurugan, P. Aruna, S. Ganesan, Determination on the binding of thiadiazole derivative to human serum albumin: a spectroscopy and computational approach, J. Biomol. Struct. Dyn. 35 (2017) 817-828.

60. A. Varlan, M. Hillebrand, Bovine and human serum albumin interactions with 3-carboxyphenoxathiin studied by fluorescence and circular dichroism spectroscopy, Molecules 15 (2010) 3905-3919.

61. S. Zhang, X. Chen, S. Ding, Q. Lei, W. Fang, Unfolding of human serum albumin by gemini and single-chain surfactants: A comparative study, Colloids Surf. A Physicochem. Eng. Asp. 495 (2016) 30–38.

Novel piperonal 1,3,4-thiadiazolium-2-phenylamines mesoionic derivatives: Synthesis, tyrosinase inhibition evaluation and HSA binding study

Natália Drumond Lopes,[†] Otávio Augusto Chaves,[†] Márcia C. C. de Oliveira, Carlos Mauricio R. Sant'Anna, Danilo Sousa-Pereira, José Carlos Netto-Ferreira,[*] Aurea Echevarria,[*]

Departamento de Química, Universidade Federal Rural do Rio de Janeiro, Rodovia BR-465, Km 7, 23970-000, Seropédica/RJ, Brazil

Highlights

*Novel mesoionic derivatives were synthesized, tested against tyrosinase and studied its interaction with HSA.
***PMI-5** and **PMI-6** can inhibit the tyrosinase activity, however **PMI-5** is the most active - IC_{50} = 124 µmol L^{-1}.
***PMI-5** and **PMI-6** interact moderately with HSA. Sudlow's site I is the main binding site.
*From the CD results, **PMI-5** and **PMI-6** are able to destroy the hydrogen bonding network of albumin.

Graphical Abstract

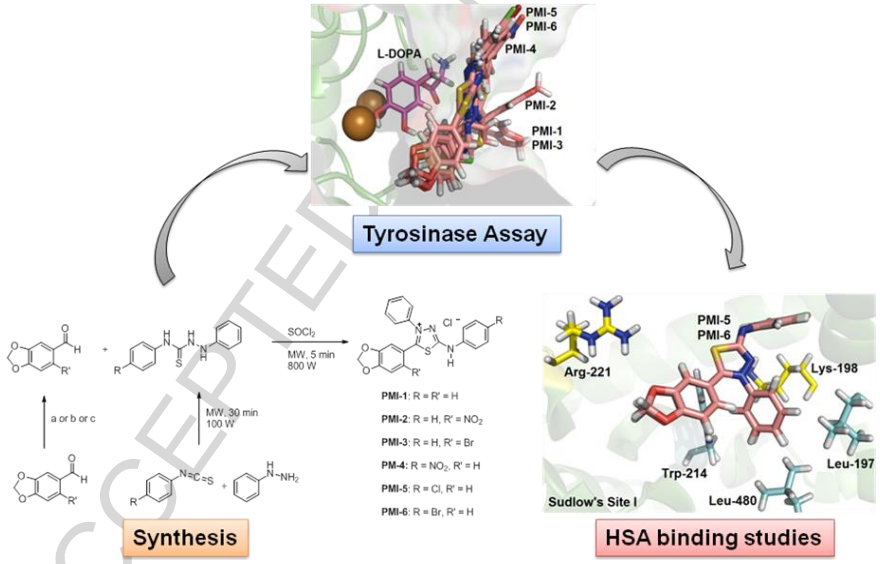

* Corresponding authors.
E-mail addresses: jcnetto.ufrrj@gmail.com (J.C.Netto-Ferreira),
echevarr@ufrrj.br (A. Echevarria).